Effects of Mn Content on Recrystallization Behavior and Texture Evolution of 3xxx Al Alloy

CHUNG-YI YU*, JUNG-PANG CHANG, SHI-XUAN DING*, TIEN-YU TSENG* and HAN-CHENG SHIH***

**New Materials Research & Development Department, China Steel Corporation*
***Research & Development Department, China Steel Aluminum Corporation*

Recrystallization behavior and texture evolution of AA3104 beverage can body stock with various Mn contents were investigated by proper combination of the thermomechanical process simulator (Gleeble 3800) and heat treatment. The result shows that the incubation time of recrystallization was shortened but the recrystallized grain growth rate was decelerated with increasing the Mn contents. The behavior could be interpreted via the Particle Stimulated Nucleation (PSN) effect during the incubation period and the pinning force of solute Mn at growth. As for texture evolution, the intensity of the cube component exhibits an evidently dependence on the number of particles with a diameter larger than the critical value d_c. The number of these "active" particles increases with the level of Mn content before recrystallization results in the reducing of the intensity of the Cube component. The phenomenon could be explained quantitatively in terms of the criterion recommended by Humphreys.

Keywords: Mn contents, Recrystallization, Texture evolution, Cube component

1. INTRODUCTION

AA3104 Al alloy, containing Mn as a main alloying element, is widely used in the beverage can industry. Because of tough competition in this market, can manufacturers are exerting every effort to develop the highly metallurgical quality can body stock, and to refine the fabrication process for cost reduction. One of the most important properties of the beverage can is of the crystallographic anisotropy[1-4], which results in the formation of ears on the cup rim after drawing. These ears are accentuated by an ironing process and have to be trimmed before further processing. Hence, they constitute the material wastage.

The ears of the final gauge sheet are regularly exhibited at 45/135^o with respect to rolling direction. This phenomenon is generally attributed to the strong rolling (deformation) texture developed during cold rolling. An industrial solution to diminish the height of these protrusions is to enlarge a sufficient amount of the Cube texture, which promotes 0/90^o earing, through fully recrystallization after hot rolling. As a consequence, a minimum earing can be achieved by the counterbalance between the deformation and recrystallization textures[3-6].

It has been reported that AA3104 Al alloy is usually of a bimodal distribution of intermetallics consisting of coarse primary constitute particles produced at the solidification stage and fine dispersoids precipitated in the following thermomechanical process[1-4,7]. The size distribution and the volume fraction of the intermetallic particles are very vital factors in controlling the recrystallization behavior and the texture evolution for the hot-rolled material. Coarse particles (> 1μm) can act as sites for promoting recrystallization, namely Particle Stimulated Nucleation (PSN)[8-10], whereas fine dispersoids can retard recrystallization by pinning the grain/subgrain boundaries via Zener drag[2,7,8].

Elemental Mn of AA3104 Al alloy also has a significant influence on recrystallization and texture. Most attention has been paid to the effects of constitute particles and dispersoids bearing Fe and Si[1-4], however, the understandings of effect of Mn contents on the recrystallization and texture is still limited. Thus, the various Mn contents were introduced into AA3104 Al alloy by a proper combination of DC (Direct Chill) casting and homogenization treatment. After hot deformation, the recrystallization kinetics as well as the texture evolution was investigated by means of the heat treatment in this study. The solid solution effect of atom Mn was clarified in this study as well. In addition, the mechanism of Cube texture development was analyzed quantitatively.

2. EXPERIMENTAL METHOD

In this study, AA3104 Al sheet slabs composed of different Mn concentrations were manufactured by DC casting. The chemical compositions were listed in Table 1. The slabs were machined into a rectangle of 38 mm in width by 25 mm in length and 15 mm in thickness, with the longitudinal side parallel to the casting direction. Meanwhile, in order to clarify the solid solution effect after hot tandem rolling, the specimens were homogenized at 600°C isothermally for 24 h for preparing the different level of Mn element in solid solution.

Plane Strain Compression (PSC) tests were executed by the use of a Gleeble 3800 thermomechanical process simulator to simulate the industrial hot tandem rolling operations. It can be programmed to simulate both thermal and mechanical industrial process variables for a wide range of hot deformation conditions. The specimens were uniaxial multi-compressed to a total true strain of 2.4 at 360°C under a constant strain rate of 50 s^{-1}. In all PSC tests, the graphite foils were used at the anvil-platen/specimen interface as a lubricant to reduce friction. All specimens were heated to deformation temperature at the rate of 5 °C/s, and held for 90 s at the temperature prior to compression. After deformation, the specimens were cooled via compressed air for the following microstructural experiments. The quenched specimens were then annealed in a salt bath at 340°C for various lengths of time and quenched so that the static recrystallization kinetics could be metallographically determined. Electron Back Scattering Diffraction (EBSD) was adopted to quantify the percentage recrystallized in each specimen. EBSD mapping acquired by automatic scanning with steps (pixel size) of 2 μm was carried out using a Field Emission gun Scanning Electron Microscope (FESEM) equipped with a HKL Channel 5 system.

The annealed specimens were mounted, polished, and anodized using Barker's reagent so that the microstructure evolution could be examined optically. In addition, the particle morphologies and distributions before and after hot compression specimens were observed by means of the FESEM as well.

The amount of solid solution can be deduced in accordance with electrical conductivity measurement that expressed as a percent of the International Annealed Copper Standard (IACS). In AA3xxx Al alloys, only very small concentrations of Fe and Si are in solid solution and it has been reported that their concentrations vary little during heat treatment[1]. Mn is the main contributor to the electrical conductivity in these alloys. Thus, the electrical conductivity could be transferred into the amount of Mn in solid solution by the empirical equation referenced from the CSC interior report[11].

The crystallographic texture measurement was measured on the compression plane by the use of X-ray diffractometer. Four incomplete pole figures, namely {111}, {200}, {220} and {311} were measured at mid-thickness by the Schulz reflection method using Mo Kα radiation[12]. Orientation distribution functions (ODFs, f(g)) were subsequently computed with series expansion method (l_{max}= 22) from the experimental pole Figures[12]. The orientations are expressed in the form of a triple of Euler angles (ϕ1, Φ, ϕ2) according to Bunge's notation[8,12].

The specimens for Transmission Electron Microscope (TEM) observation were mechanically thinned down to about 75 μm in thickness and final polished with a standard twin-jet polishing method using an electrolyte of 25% nitric acid and 75% methanol at -30°C and 15 V. The microstructural characterization was carried out in a Joel 100CX TEM operated at 100 kV.

3. RESULTS AND DISCUSSION

Homogenization effect on the microstructural evolution of the as-cast AA3104Al alloy was observed by SEM, as shown in Fig.1. It exhibits a typically continuous network or script-like morphology of the primary constituent particle (Fig.1a) in as-cast condition. After 600°C 24 h heat treatment, the constituent particles have been spheroidized and most of them have been broken up into smaller fragments (Figs 1b, c, and d). The primary particle sizes also coarsen with increasing the concentration of Mn. Besides, the electrical conductivity shows a strong dependence on the Mn contents (Table 2), which might be ascribed to the limitation of Si contents[1] (Table 1).

Table 1 Chemical compositions of AA3104 Al alloys used in this study (wt%)

Sample code	Si	Fe	Mn	Mg	Al
L Mn	0.22	0.44	0.49	1.19	Bal.
S Mn	0.23	0.46	0.88	1.20	Bal.
H Mn	0.21	0.43	1.21	1.15	Bal.

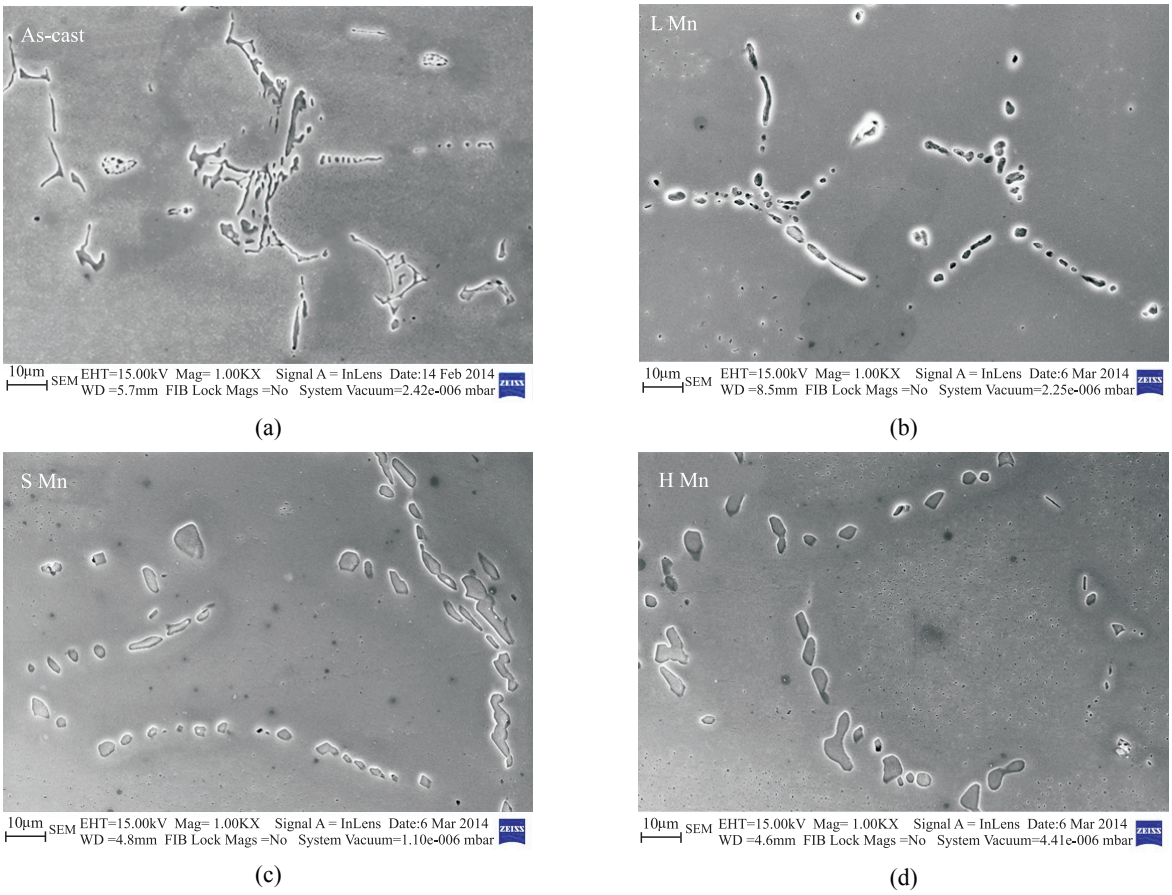

Fig.1. SEM micrographs showing the morphology of the primary constituent particle before (a) and after homogenization (b) L Mn (c) S Mn and (d) H Mn.

Table 2 Electrical conductivity and their corresponding concentration Mn in solid solution after homogenization at 600°C 24 hours

Sample	IACS%	Concentration of Mn in solid Solution (wt%)
L Mn	40.5	0.28
S Mn	37.2	0.38
H Mn	34.7	0.47

The major phase of the as-cast AA3104 Al alloy (S Mn) is the orthorhombic $Al_6(Fe, Mn)$ as shown in Fig.2a. The other minor cast phase cubic α_c-$Al_{12}(Fe, Mn)_3Si$ (α_c), generally reported by literature[1], was not investigated in this specimen.

After homogenization, however, the $Al_6(Fe, Mn)$ phase has transformed into α_c phase as shown in Fig.2b. Simultaneously, dispersoid particles of the α_c, usually around two orders of magnitude smaller than the constituents, precipitate from the supersaturated Al matrix within grain interiors. A bimodal distribution composed of both kinds of particles aforementioned has a profound effect on the microstructural development and in particular recrystallization behavior during subsequent processing. Additionally, the intensity of the transformed α_c phase among specimens has a little discrepancy due to the limitation of Si content. But the XRD peaks of the $Al_6(Fe, Mn)$ phase develop stronger gradually with increasing the concentrations of Mn (Fig.2b). Obviously, the increasing Mn concentrations seem to have a benefit for the development of $Al_6(Fe, Mn)$ phase.

Generally, PSC tests were used to simulate the microstructural evolution of the hot tandem rolling. Typically as-PSCed microstructure was observed via POM (Polarization Optical Microscope) as present in Fig.3a. It reveals a deformed structure with elongated grain morphology along the longitudinal direction. Figure 3b

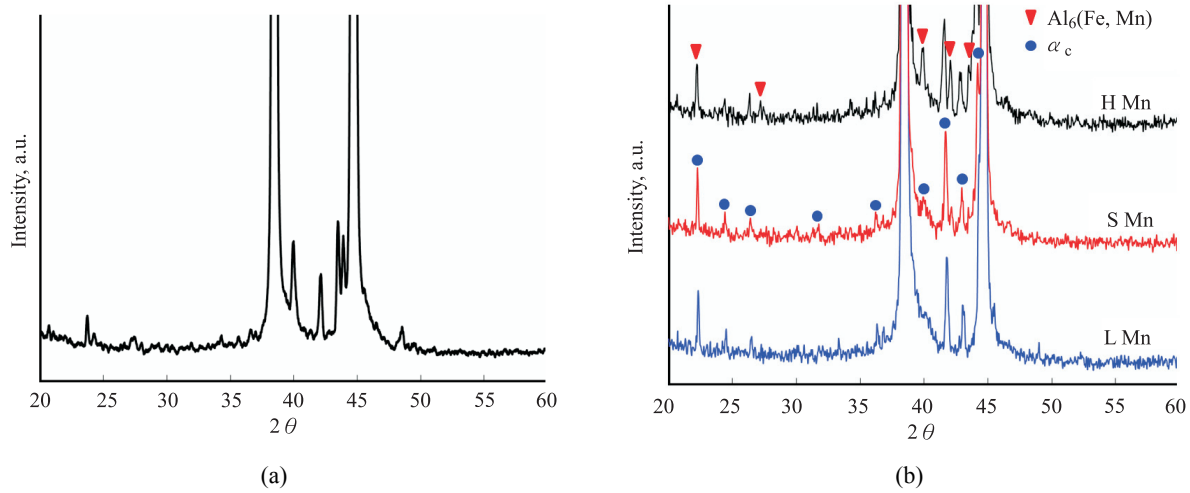

Fig.2. XRD identification (a) before and (b) after homogenization.

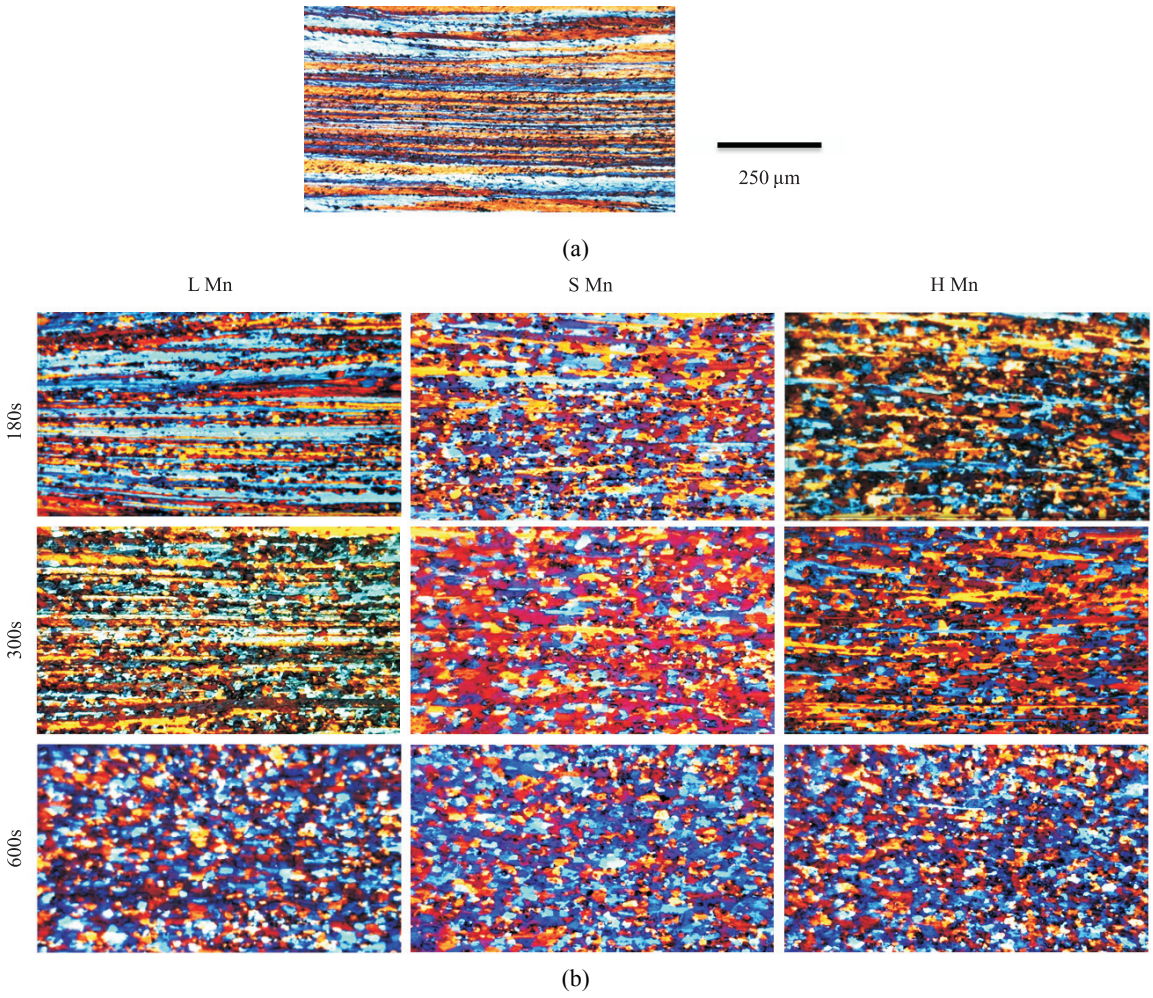

Fig.3. (a) Polarization optical micrograph showing the typically elongated grain structure in the as deformed specimens, (b) Evolution of the microstructure with increasing annealing time.

shows representative microstructures of selected specimens that annealed isothermally at 340°C with different lengths of time. The corresponding volume fraction recrystallized (Xv) was evaluated by the use of the EBSD as shown in Fig.4. According to the experimental results, the specimen H Mn exhibits the largest Xv value at initial state of 180 s. With annealing time increased to 300 s, the specimen L Mn still

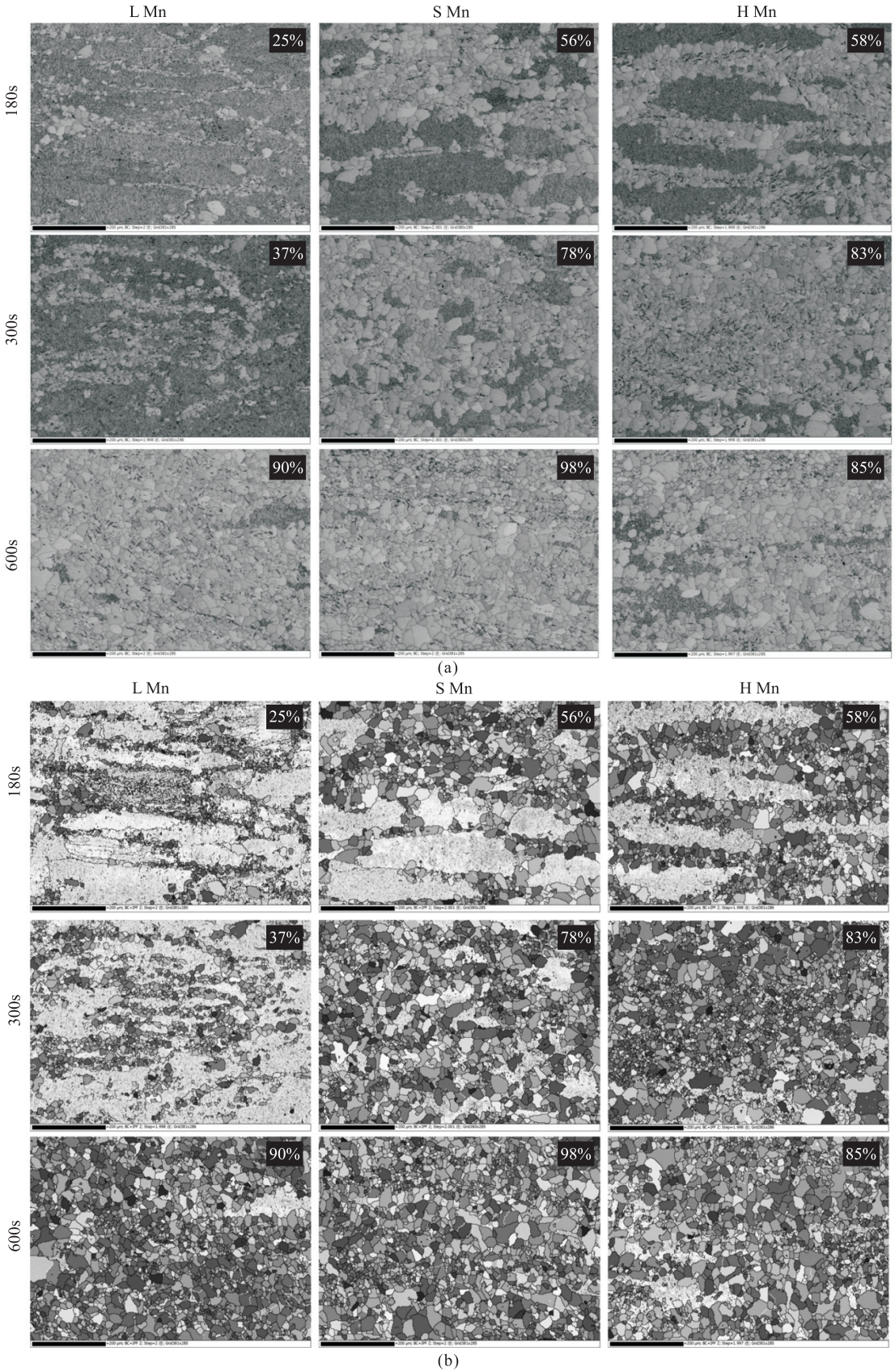

Fig.4. Development of volume fraction recrystallized (Xv) with increasing annealing time. (a) Band contrast maps and (b) OIM orientation maps.

presents lots of deformed structure as compared with the other two specimens. As the annealing time was up to 600 s, only the Xv value of specimen S Mn could be regarded as fully recrystallization. It is worth of noting that the Xv value of specimen L Mn is larger than that of specimen H Mn after 600 s annealing. The dependence of Mn contents upon recrystallization kinetics of AA3104 Al alloy annealed at 340°C is shown in Fig.5. Specimen H Mn shows the shortest incubation time of all, however, its velocity of recrystallization kinetics decreases with extending the annealing time. In contrast to specimen H Mn, the specimen L Mn exhibits an entirely different recrystallization behavior. It has lower nuclei density (Fig.5) resulted from the prolonged incubation period, which causes the recrystallized rate to fall far behind the other two specimens as the Xv value beneath 50%. Nevertheless, the fully recrystallization of specimen L Mn could be accomplished as a consequence of the acceleration of the boundary mobility as the Xv value is over 50%.

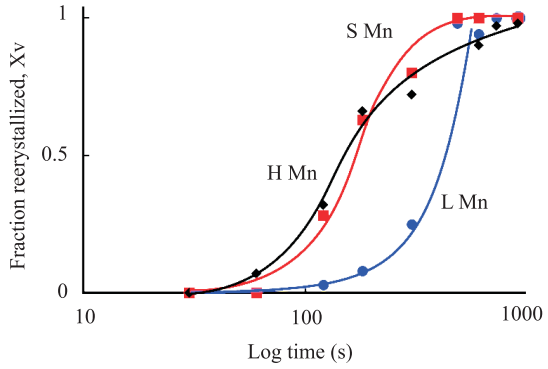

Fig.5. The recrystallization kinetics of AA3104 Al alloy with different Mn contents annealing at 340°C with different lengths of time.

Figure 6 shows the SEM observations of as-PSCed specimen before heat treatment. There is little discrepancy in particle size (> 1 μm, not secondary precipitates) among all conditions. The particle density, thus, increases with the level of Mn. From the literature reports[8-10], the mobile dislocations tend to be trapped by undeformable particles upon deformation. The dislocation density tangled around the particles increases dramatically, which is higher than that in grain interior. As a result, it is easy to stimulate nucleation adjacent to the particle (PSN effect). Therefore, the particle density of specimen H Mn is the highest that exhibits the shortest incubation period.

On the other hand, the amount of solid solute Mn atom in matrix increases obviously with the Mn contents (Table 2). In General, the solid solute atom

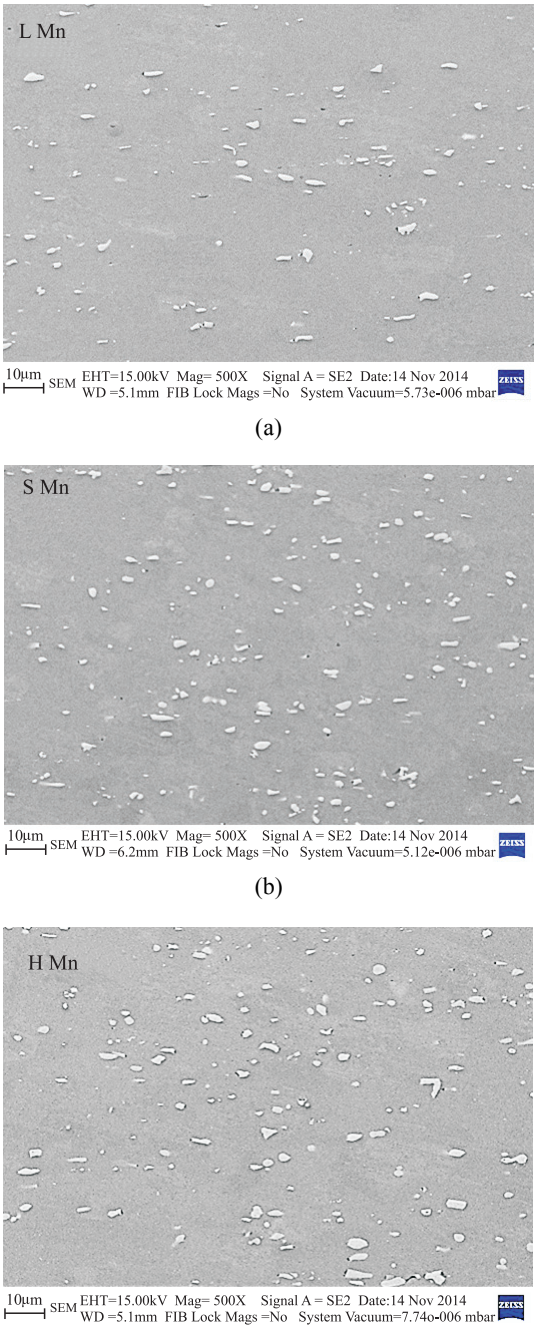

Fig.6. SEM micrographs showing the particle distributions of as-PSCed specimens before annealing; (a) L Mn, (b) S Mn and (c) H Mn.

exerts a retarding force on grain boundaries and reduces their migration velocity enormously. Consequently, the growth rate of recrystallizing grains has been diminished. In this study, the amount of solid solute of specimen H Mn is the highest that demonstrates the strongest drag force. It causes the recrystallized grain growth rate of specimen H Mn to decelerate

with annealing time. For the specimen contains the lowest concentration, however, solute Mn has little influence on the boundary mobility[8]. There is no any interference in the period of recrystallization. The recrystallized nucleus boundaries could be migrated at a faster speed in contrast to specimen H Mn. As regards to the moderate Mn content (S Mn), it takes the least time path in average for achieving fully recrystallization as seen from the Figs 5 and 6. It might be ascribed to the dynamic equilibrium of the recrystallized grain boundary migration rate and drag force of solid solution Mn.

Figure 7a shows the influence of the various Mn concentrations on the recrystallization texture evolution by isothermal annealing at 340°C for different lengths of time. It is noted that the evolution of recrystallization texture depends strongly on the Mn concentrations. As shown in Fig.7a, the as deformed specimen exhibit the typical rolling texture composed of the α fibre[8,12], which is characterized by the development of preferred orientations along the Goss component G {011}<100> to the Brass component Bs {011}<211>. After annealing up to 300 s, the intensity of the Cube component {001}<100> increases with the Mn concentrations. A sharp Cube component has dominated after annealing for 600 s, but there is still some minor intensity of residual rolling textures. Figure 7b shows the f(g) values after fully recrystallization by plotting the intensity from the exact Cube component along ϕ towards the G component. Specimen L Mn exhibits the highest intensity of Cube component of all, however, the other two specimens (S Mn and H Mn) exhibit limited discrepancy.

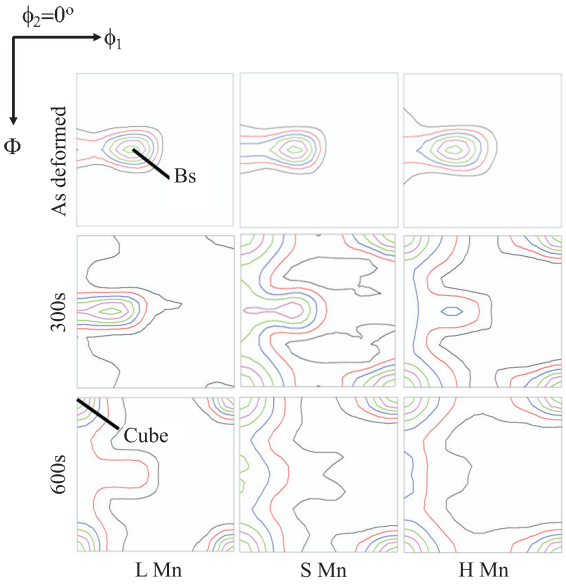

(a)

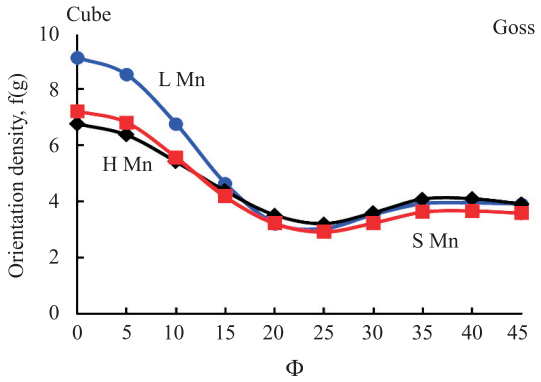

(b)

Fig.7. (a) Influence of the various Mn concentrations on the recrystallization texture evolution by isothermal annealing at 340°C for different lengths of time and (b) Intensity from the exact Cube component along ϕ towards the G component of the specimens after fully recrystallization varying with different Mn contents.

Evolution of the recrystallized texture in AA3104 Al alloy with a bimodal particle distribution might be interpreted by the criterion recommended by Humphreys[2,3,7,8]. It is based on the concept of competing process for nucleation of recrystallized grains having different orientations. The particle density capable of stimulating nucleation of recrystallization is considered to be the essential factor responsible for the texture variation, i.e. a high density of active particles result in weak texture (random texture) and low Cube intensity. To act as a potential nucleation site for PSN, therefore, a particle size must exceed a critical diameter d_c to overcome the Gibbs-Thompson effect[13], which is given by

$$d_c \geq \frac{4\ell\gamma_{gb}}{3\gamma_{sb} - 2\ell Z} \quad \text{.....(1)}$$

where l is the subgrain size, γ_{gb} and γ_{sb} are energies of the grain boundaries and subgrain boundaries respectively, and Z is the Zener pinning pressure. According to the Shockley-Read equation, the grain boundary ratio γ_{sb}/γ_{gb}= 0.3 was used for estimation in this study[3,7,14]. For a volume fraction F_v of secondary precipitates of diameter D, then the Zener pinning pressure is

$$Z = 3F_v/D \quad \text{.....(2)}$$

In order to simplify the equation and more convenient for experiment measurement, the Zener pinning pressure on the boundary can be written as[2,3]

$$Z = N_A \pi \bar{\gamma} \gamma_{gb} \quad \text{.....(3)}$$

where N_A is the number of the particles per unit area and $\bar{\gamma}$ is the average particle radius.

The values of critical particle diameter d_c could be determined by means of the aforementioned equations. Through introducing the d_c as a threshold in the size distribution, the number of particles with a diameter larger than d_c was obtained as shown in Table 3. It is associated with the number of "active" particles for stimulating non-Cube oriented recrystallized grains. As a result, the intensity of the cube component exhibits an evidently dependence on the number of particles with a diameter larger than d_c. The Mn content directly affects the frequency of coarse particles. A reducing Mn content as well as lower solid solution gives rise to a strengthening of the Cube texture (Tables 2 and 3). It appears to imply that a weakening drag force on grain boundary has a benefit to the development of the Cube orientated nuclei upon the recrystallization period.

Table 3 Influence of the number of particles with diameter larger than d_c on the intensity of Cube component

Sample	l	d_c	No. particles > $d_c/\mu m^2$	Cube component intensity, f(g)
L Mn	0.60	3.3	139	~9.2
S Mn	0.59	3.4	198	~7.1
H Mn	0.56	3.3	210	~6.8

4. CONCLUSIONS

1. Various Mn contents have a great influence on the recrystallization behavior of the PSCed specimens during annealing. With increasing the Mn content, the incubation period has been shorten as a results of the PSN effect impelled by a larger quantity of coarsen particles, however, its recrystallization growth rate is decelerated that could be attributed to the retarding force of the higher amounts of solid solute Mn in the matrix.
2. For the specimen with the lowest Mn content, the solute Mn has little influence on the boundary mobility results in the recrystallized boundaries migrating at a faster speed as volume fraction recrystallized over 50%.
3. Evolution of recrystallization texture for PSCed specimens during annealing shows a strongly dependence on the Mn concentrations, i.e. the intensity of Cube component increases with decreasing the Mn content.
4. Evolution of the recrystallized texture in AA3104 Al alloy with a bimodal particle distribution could be interpreted quantitatively based on the criterion recommended by Humphreys.
5. The Mn content directly affects the frequency of coarse particles for AA3104 Al alloy. As the Mn content increases, the number of active particles, thus, the number of particles with diameter larger than d_c, tends to stimulate the non-Cube oriented recrystallized grain. As a result, the intensity of the Cube orientation has been diminished.

REFERENCE

1. J. G. Morris, H. D. Merchant and E. J. Westerman, Aluminum Alloys for Packaging, TMS, 1992, p.1.
2. H. D. Merchant, J. Crane and E. H. Chia, Homogenization and Annealing of Aluminum and Copper Alloys, The Metallurgical Society, Inc., 1988.
3. W. B. Hutchinson, A. Oscarsson and Å. Karlsson, Mat. Sci. Tech., 1989, vol. 5, p. 1118.
4. W. B. Hutchinson and H. E. Ekström, Mat. Sci. Tech., 1990, vol. 6, p. 1103.
5. G. J. Marshall, Mat. Sci. Forum, 1996, vol. 217-222, p. 19.
6. R. K. Bolingbroke and G. J. Marshall, Mat. Sci. Forum, 1993, vol. 113-115, p. 685.
7. E. H. Chia and H. J. McQueen, Microstructural Control in Aluminum Alloys: Deformation, Recovery and Recrystallization, AIME, 1985.
8. F. J. Humphreys and M. Hatherly, Recrystalliation and Related Annealing Phenomena, Pergamon, 1995.
9. H. M. Chan and F. J. Humphreys, Acta Metal., 1984, vol. 32, no. 2, p. 235.
10. F. J. Humphreys, Acta Metall., 1977, vol. 25, p. 1323.
11. C. Y. Yu, China Steel Report (PJ01679), 2012.
12. V. Randle and O. Engler, Introduction to Texture Analysis: Macrostructure, Microstructure and Orientation Mapping, CRC Press, 2000.
13. D. A. Portor and K. E. Easterling, Phase Transformations in Metals and Alloys, Second Edition (Chapman & Hall), 1992.
14. S. Benum and E. Nes, Acta Metal., 1997, vol. 45, no. 11, p. 4593. □